

Article

Evaluation of the Success of Simulation of the Unmanned Aerial Vehicle Precision Landing Provided by a Newly Designed System for Precision Landing in a Mountainous Area

Pavol Kurdel , Natália Gecejová , Marek Češkovič *  and Anna Yakovlieva 

Faculty of Aeronautics, Technical University of Košice, Rampová 7, 041 21 Košice, Slovakia

* Correspondence: marek.ceskovic@tuke.sk; Tel.: +421-55-602-6149

Abstract: Unmanned aerial vehicle technology is the most advanced and helpful in almost every area of interest in human work. These devices become autonomous and can fulfil a variety of tasks, from simple imaging and obtaining data to search and rescue operations. The most challenging environment for search and rescue operations is the mountainous area. This article is devoted to the theoretical description and simulation tests of a prototype method of landing the light and the medium-weight UAVs used as supplementary devices for SAR (search and rescue) and HEMS (helicopter emergency medical service) in hard-to-reach mountainous terrains. The autonomous flight of a UAV in mountainous terrain has many specifics, and it is usually performed according to predetermined map points (pins) uploaded directly into the control software of the UAV. It is necessary to characterise each point flown on the chosen flight route line in advance and therefore to know its exact geographical coordinates (longitude, latitude and height of the point above the terrain), and the control system of UAV must react to the change in the weather and other conditions in real time. Usually, it is difficult to make this forecast with sufficient time in advance, mainly when UAVs are used as supplementary devices for the needs of HEMS or MRS (mountain rescue service). The most challenging phase is the final approach and landing of the UAV, especially if a loss of GNSS (global navigation satellite system) signal occurs, like in the determined area of the Little Cold Valley in the Slovak High Tatras—which is infamous for the widespread loss of GNSS signals or communication/controlling connection between the UAV and the pilot-operator at the operational station. To solve the loss of guidance, a new method for guiding and controlling the UAV in its final approach and landing in a determined area is tested. An alternative landing navigation system for UAVs in a specific mountainous environment—the authors' designed frequency Doppler landing system (FDLS)—is briefly described but thoroughly tested with the help of artificial intelligence. An estimation of dynamic stability is used based on the time recording of the current position of the UAV, with the help of a frequency-modulated or amplitude-modulated signal based on the author's prototype of a precision landing system designed for mountainous terrain. This solution could overcome the problems of GNSS signal loss. The presented research primarily evaluates the success of the simulation flights for the supplementary UAV. The success of navigating the UAV to land in the mountainous environment at an exact landing point using the navigation signals from the FDLS was evaluated at more than 95%.

Keywords: evaluation of successful landing; mountain environment; precious landing; simulation; UAV



Citation: Kurdel, P.; Gecejová, N.; Češkovič, M.; Yakovlieva, A. Evaluation of the Success of Simulation of the Unmanned Aerial Vehicle Precision Landing Provided by a Newly Designed System for Precision Landing in a Mountainous Area. *Aerospace* **2024**, *11*, 82. <https://doi.org/10.3390/aerospace11010082>

Academic Editor: Gokhan Inalhan

Received: 12 December 2023

Revised: 8 January 2024

Accepted: 15 January 2024

Published: 16 January 2024



Copyright: © 2024 by the authors. Licensee MDPI, Basel, Switzerland. This article is an open access article distributed under the terms and conditions of the Creative Commons Attribution (CC BY) license (<https://creativecommons.org/licenses/by/4.0/>).

1. Introduction

Systems providing fully automated guidance of an aircraft for precision landing are standard and mandatory equipment at airports with 24-h operations worldwide [1]. Navigation of the helicopters and the aeroplanes to the runway threshold using ILS (instrument landing system) and MLS (microwave landing system) precision landing systems are based

on comparing a pair of amplitude-modulated signals. The observable is also an expansion of the use of GNSS signals for augmentation systems such as satellite-based augmentation systems (S-BAS), ground-based augmentation systems (G-BAS) or differential global positioning systems (DGPS), which are widespread worldwide but are hardly usable for UAVs, especially those intended for use in mountain environments for search and rescue (SAR) purposes, as well as medical delivery (supplementary UAVs for HEMS) [2,3]. An option is a controlled landing by a pilot-operator who, after the initial autonomous flight, would take control during the final phase of the approach to landing (approx. at a 60 m flight height above the terrain). To land the UAV at the final destination point, in addition to direct visual contact, he would also use the conventional equipment of the UAV—acoustic sensors, sensors working in the visible and infrared spectrum, and possible information from the inertial navigation unit [4]. A pilot-operator-controlled landing approach is not optimal, mainly because the pilot-operator needs continuous contact with the UAV. Ideally, he would have to be near the injured person requiring assistance, which is an unrealistic condition for providing flight of the UAV, especially in mountainous and hard-to-reach terrains. Considering that, it is necessary to realise not only a fully automated flight but also fully automated landing of UAVs, especially in a specific high mountain area in which the signal from GNSS satellites is missing and any other control or navigation signals could interfere with the surrounding forested and mountainous environment. It is necessary to navigate the UAV to the landing point (threshold) and provide precision landing with the help of a modified landing system with specially designed and modified software—which is the subpart of the presented research [5–7].

During the flight (life-saving) missions of unmanned aerial vehicles, as part of the solution for the self-navigation of the UAV in the landing phase, it is necessary to take into account the constant dynamic change in the lateral deviations of the UAV (influence of the wind and the windward and leeward sides of the mountain massif), the specifics of the chosen flight mission or the changing dynamics of the UAV during the flight caused by transportation of medication, adrenaline pens or a defibrillator [8]. Considering the above, environmental and atmospheric errors of the UAV's automated flight should be taken into account and monitored as part of the passive adaptation in the UAV's landing mode (phase) [9–13]. All of the mentioned aspects are considered by the frequency Doppler landing system (FDLS) designed by the authors' team for a precise approach and landing of the UAV in the mountainous area/massif (Figure 1).

The use of the acoustic spectrum to detect the presence of the unmanned aerial vehicle in the monitored area is familiar. Such detection of the presence of UAVs primarily fulfils a security purpose, and it serves to protect the fauna, flora, health and property of the state, legal entities and natural persons, as well as to ensure a safe flight area in the monitored area [14–16]. The disadvantage of using the acoustic spectrum in the mountains is the high refraction of the signal from surrounding obstacles (rocks, trees and other objects). For this reason, the authors' FDLS, using radio signals, was chosen as a navigation element for UAV landing in this environment. Moreover, this is also thanks to highly positive experiences in previous research [17].

For the new application possibilities of precise UAV landing in the mountain massif, which is the subject of the presented research, the landing Doppler system working on the frequency principle designed by the authors can be used (Figure 1, Section 2). This system provides a direct connection between the frequency band and the generation of the Doppler frequency (shift), arising when the UAV approaches the proposed landing system for the UAV. The designed and tested landing Doppler frequency range is several hundred meters under standard conditions (the negligible reflections of radio waves from the surrounding environment). Measurements and simulations for acquiring the ideal characteristics for the precision landing system FDLS for landing UAVs in the massif were carried out in laboratory conditions, with the findings transformed into the real form of the landing system (Figure 2).

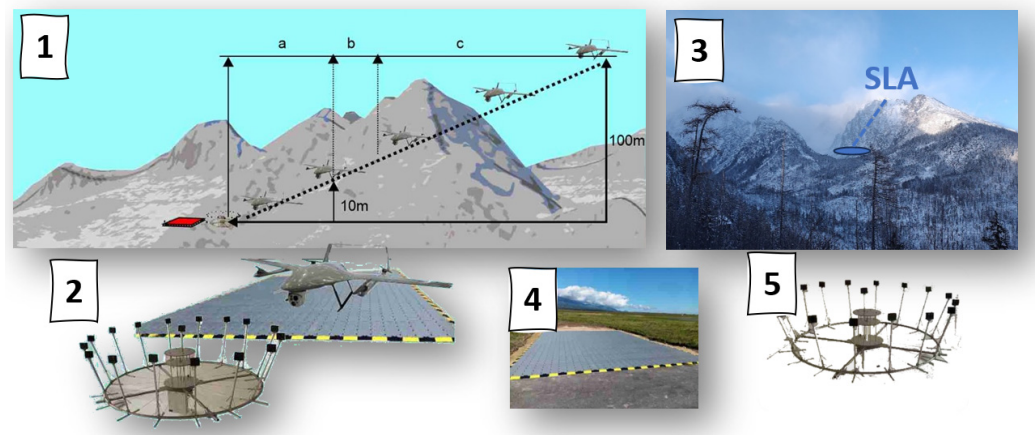


Figure 1. Graphic representation of the research problem. (1). Determined research area—the Little Cold Valley, High Tatras, Slovak Republic: (a) area with loss of GNSS signal; navigation of the UAV for approach and landing only with navigation information from the frequency Doppler landing system (FDLS); (b) area with available navigation information from GNSS satellites combined with navigation information from the FDLS; (c) area with stable GNSS signal. (2). Authors’ design of the FDLS for UAVs, usable in mountainous environment. (3). The reference point (successful landing area) for experimental flight tests of UAV landing with the navigation signals from the FDLS in the mountain massif. (4). Experimental landing area for UAV landing using the FDLS. (5). The experimental FDLS is designed for UAV landing in mountain areas.

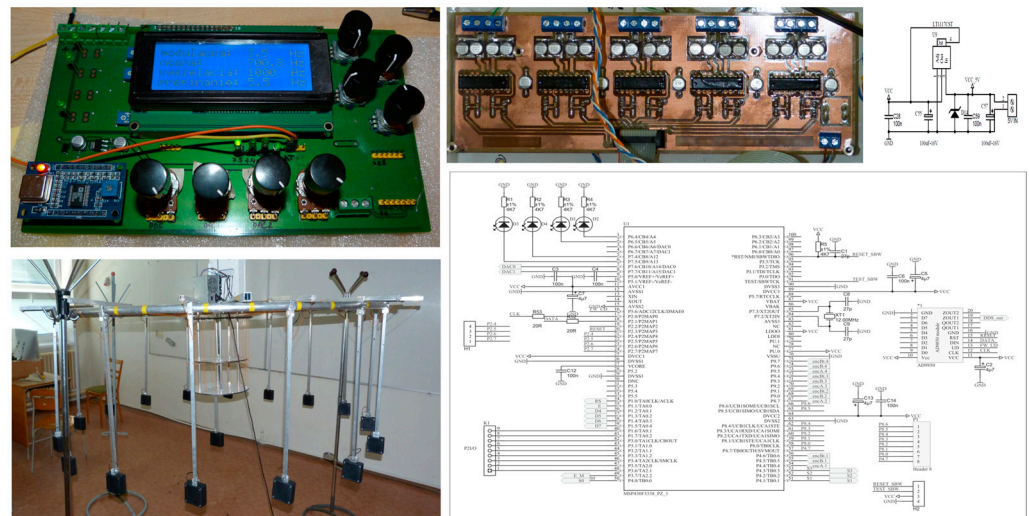


Figure 2. Frequency Doppler landing system designed for landing the UAV in mountainous areas.

For the FDLS, the equivalent of the reference signal is a low-frequency amplitude-modulated signal. To the best possible effect, it is advisable to ensure the possibility of changing the frequency and amplitude of the signal. Because the system is designed in the radio band, the range of carrier frequencies is determined from 88 MHz to 500 MHz. The modulation frequency is theoretically determined from 30 Hz to 511 Hz. Experimental measurements confirmed these values in the laboratory and later in simulation conditions. Sixteen electronically switchable transmitters create a frequency-modulated signal at the reception point, while their switching frequency is synchronised with the modulation frequency. Due to the components used and the overall concept of the electronic part, it is possible to select individual frequencies for the final functionality of the system. The used microcontroller works with a frequency of 12 MHz, and the sampling frequency of the used analogue converter is 32 kHz, thanks to which the necessary frequency range of

the system is covered (from 88 MHz to 500 MHz). The output power of the amplifiers at 12 V supply voltage and 4 Ω load, excited by a harmonic signal of 511 Hz, is 2.85 W.

During simulation flight experiments, it was proven that reflections occur in the mountain massif, but they can be reliably filtered out with a high-precision filter of concentrated selectivity. It was also proven that the emergence of the necessary Doppler effect was significant and could be used for precise landing of the UAV in a mountainous environment, already at a distance of several hundred meters (experimentally verified accuracy reached the level of 3000 m). It has been proven that using the newly designed frequency Doppler navigation device for precise UAV landing is possible and reliable.

The process of connecting (coherence) the automated flight of the UAV in the mountain environment with its automated final landing at the reference point, SLA, with the navigation signals from the frequency Doppler landing system is described in the chapter focused on Methodology and Measurement.

2. Methodology and Measurement

A precise, fully automated UAV landing during standard conditions (accessible terrain, satisfactory atmospheric and meteorological conditions) can be performed if the navigation system and control software perform their functions correctly. However, this method of landing does not solve the problems associated with the failure of the conventional UAV landing system, possible problems associated with the loss of navigation signals from GNSS satellites, or interference or multipath in the propagation of navigation signals during UAV flights in the mountains, which represent a complicated landing situation [17–19].

The strategy of simulation testing, described in Section 2.1 and subsequent evaluation of simulated flights devoted to the third chapter, was chosen for the relevant solution to the established problem.

2.1. Reliability and Flight Dynamics of the Chosen UAV in a Specific Mountain Area—The Base for Simulation and Evaluation of the Success of the UAV Flights and Precise Landings

Considering the initial financial costs, the DJI Mavic Pro, equipped with a conventional sensor and avionics equipment supplemented with an experimental onboard Doppler landing receiver, was chosen as the research object for simulation testing and later planned testing in real conditions.

The mathematical model of the chosen unmanned aerial vehicle was created based on the general motion Equations (1)–(10) for a quadcopter [20–24] (Figure 3).

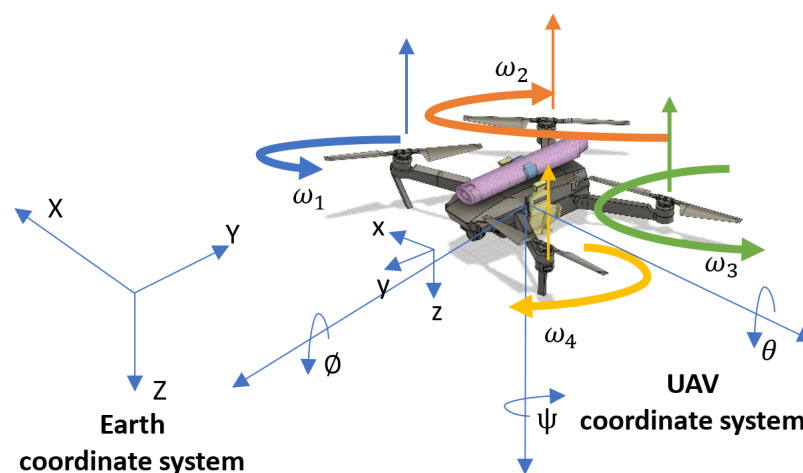


Figure 3. Representation of the movement and rotation axis of the quadcopter DJI Mavic Pro, equipped with an adrenaline pen.

The movement of the UAV can be expressed in four basic movements, the change in altitude a_1 , roll a_2 , pitch a_3 and yaw a_4 , which are given as follows in Equations (1)–(4):

$$a_1 = k_t (\omega_1^2 + \omega_2^2 + \omega_3^2 + \omega_4^2) \quad (1)$$

$$a_2 = k_t (\omega_2^2 + \omega_4^2) \quad (2)$$

$$a_3 = k_t (-\omega_3^2 + \omega_1^2) \quad (3)$$

$$a_4 = k_m (\omega_1^2 - \omega_2^2 + \omega_3^2 - \omega_4^2) \quad (4)$$

where:

a_1 —is the change in altitude;

a_2 —is the change in roll;

a_3 —is the change in pitch;

a_4 —is the change in yaw;

k_t —is the aerodynamic thrust coefficient;

k_m —is the torque moment coefficient;

ω —is the angular speed of the propeller.

The mathematical model of the UAV could be created from Equations (5)–(10), expressing the movement in each axis of the Earth and body frame (UAV) coordinate system:

$$\ddot{x} = \frac{-1}{m} [k_{d_x} \dot{x} + a_1 (\sin \varnothing \sin \psi + \cos \varnothing \cos \psi \sin \theta)] \quad (5)$$

$$\ddot{y} = \frac{-1}{m} [k_{d_y} \dot{y} + a_1 (\sin \varnothing \sin \psi - \cos \varnothing \cos \psi \sin \theta)] \quad (6)$$

$$\ddot{z} = \frac{-1}{m} [k_{d_z} \dot{z} - mg + a_1 \cos \varnothing \cos \theta] \quad (7)$$

$$\dot{p} = \frac{-1}{M_x} [k_{r_x} p - la_2 - M_y qr + M_z qr + M_m q \omega_r] \quad (8)$$

$$\dot{q} = \frac{-1}{M_y} [-k_{r_y} q + la_3 - M_x pr + M_z pr + M_m p \omega_r] \quad (9)$$

$$\dot{r} = \frac{-1}{M_z} [a_4 - k_{r_z} r + M_x pq - M_y pq] \quad (10)$$

where:

a_1 —is the change in altitude;

a_2 —is the change in roll;

a_3 —is the change in pitch;

a_4 —is the change in yaw;

k_t —is the aerodynamic thrust coefficient;

k_d —is the thrust drag coefficient;

k_m —is the torque moment coefficient;

k_r —is the moment drag coefficient

l —is the length of the arm of the UAV;

M —is the moment of inertia;

M_m —is the moment of inertia of the motor;

m —is the mass of the UAV.

Equations (1)–(10) were, after appropriate modification and in a suitable form, implemented in the MATLAB-Simulink (2023a version) simulation environment, which represents the primary platform for simulation research, similar to the previous research of

the authors which is followed by the current presented research [17,25]. When evaluating the success of the simulation flights, in this case, the probability of the occurrence of an extraordinary situation of the UAV during the flight mission (state of the danger, emergency and catastrophic) caused by external and internal influences was also considered. A more detailed description of the statistical estimate of the probability of occurrence of an extraordinary situation is given in Section 2.2.

2.2. Probabilistic Monitoring of the Coherence of the UAV Flight and the Possibility of Its Accurate Landing at the Reference Point (SLA) in a Mountainous Area—The Base for Simulation and Evaluation of the Success of the UAV Flights and Precise Landings

In case of failure of an autonomously flying UAV's automated landing process, the pilot-operator takes responsibility for the unmanned aerial vehicle and its control. As a rule, it solves the three statistically most frequently occurring cases of failure of the chain UAV–pilot-operator. These are a state of danger, an emergency and a catastrophic state/situation arising during the flight of a UAV. These states and the coefficients can be described by Equation (11) [26–28]:

$$k_{ds} = \frac{n_{ds}}{n_{dsur}}; k_{es} = \frac{n_{es}}{n_{ds}}; k_{cs} = \frac{n_{cs}}{n_{es}} \quad (11)$$

where:

k_{ds} —is the coefficient of dangerous UAV landing situations in the mountainous area;
 k_{es} —is the coefficient of emergency situations causing failed UAV landings in the mountainous area;
 k_{cs} —is the coefficient of catastrophic situations when the UAV unsuccessfully lands in a mountainous area, which leads to its destruction;
 n_{ds} —is the number of dangerous situations during the flight of the UAV caused by the environment;
 n_{dsur} —is the number of dangerous situations caused by the surroundings of the UAV landing area in the mountains;
 n_{ds} —is the number of UAV dangerous situations in the mountainous area;
 n_{es} —is the number of UAV emergency situations in the mountainous area;
 n_{cs} —is the number of UAV catastrophic situations in the mountainous area.

The probability of the occurrence of extraordinary situations is determined by Equation (12):

$$P_{ds} = \frac{n_{ds}}{N}; P_{es} = \frac{n_{es}}{N}; P_{cs} = \frac{n_{cs}}{N}; P_t = \frac{P_{ds} + P_{es} + P_{cs}}{N} \quad (12)$$

where:

P_{ds} —is the probability of occurrence of dangerous UAV states in the mountainous area;
 P_{es} —is the probability of occurrence of emergency UAV states in the mountainous area;
 P_{cs} —is the probability of occurrence of catastrophic UAV states in the mountainous area;
 P_t —is the total probability of occurrence of an extraordinary situation of a UAV when landing in a mountainous area;
 n_{ds} —is the number of UAV dangerous situations in the mountainous area;
 n_{es} —is the number of UAV emergency situations in the mountainous area;
 n_{cs} —is the number of UAV catastrophic situations in the mountainous area;
 N —is the number of UAV flights in the mountainous area realised in the monitored time period.

The probabilistic mathematical model for the emergence of extraordinary situations during the landing of the UAV (13) is obtained after substituting Equations (11) and (12). The resulting equation has the following form (13):

$$P_{extos} = k_{ds}k_{es}k_{cs}P_t = k_tP_t \quad (13)$$

where:

P_{extos} —is the probability of occurrence of catastrophic UAV states in the mountainous area;
 k_{ds} —is the coefficient of dangerous UAV landing situations in the mountainous area;
 k_{es} —is the coefficient of emergency situations causing failed UAV landings in the mountainous area;

k_{cs} —is the coefficient of catastrophic situations when the UAV unsuccessfully lands in a mountainous area, which leads to its destruction;

k_t —is the total coefficient of UAV extraordinary situations during landing in the mountainous area;

P_t —is the total probability of occurrence of an extraordinary situation of a UAV when landing in a mountainous area.

In such a case, P_t can be interpreted as the probability of the occurrence of complex flight conditions, representing the basis for the emergence of extraordinary situations during UAV flight. The practical importance of expressing the value of the probability of the occurrence of an emergency situation of a UAV during landing also lies in the evaluation of the economic aspect of the flight and landing of the unmanned aerial vehicle, in which the mutual connection between the UAV and the pilot-operator must be taken into account. The aspect of mutual connection (intersection) can be investigated using set theory, as follows (14) [26–28]:

$$B_0 = B \cap C \quad (14)$$

where:

B_0 —is the immediate influence that affects the chain UAV–pilot-operator;

B —is the influence that affects the chain UAV–pilot-operator;

C —is the external condition affecting UAV landing in mountainous areas;

\cap —is the intersection of factors B and C , which co-occur, or when one of the conditions occurs (15):

$$C = C_1 \cup C_2 \cup \dots \cup C_n \quad (15)$$

where:

C —is the external condition affecting UAV landing in mountainous areas;

C_n —is the n -th external condition that affects UAV landing in mountainous areas;

\cup —is the unification of individual partial conditions.

If the negation is valid, i.e., the opposite states of the interaction of the UAV–pilot-operator chain, Equation (16) will have the following form:

$$\overline{B_0} = \overline{B} \cup \overline{C}; B_0 \cap \overline{B} = \emptyset \quad (16)$$

where:

$\overline{B_0}$ —is the immediate negative influence that affects the chain UAV–pilot-operator;

\overline{B} —is the negative influence that affects the chain UAV–pilot-operator;

\overline{C} —is the negative external condition affecting UAV landing in mountainous areas;

B_0 —is the immediate influence that affects the chain UAV–pilot-operator;

\cup —is the unification of individual partial conditions;

\emptyset —is the empty set.

If Equation (16) is taken into account, the resulting form of the event probability of the emergence of extraordinary situations during UAV flight can be expressed by Equation (17):

$$P(\overline{B}) = P(\overline{B}) + P(\overline{C}) - P(\overline{B} \cap \overline{C}) \quad (17)$$

where:

P —is the probability of occurrence of the extraordinary situation;

\overline{B} —is the negative influence that affects the chain UAV–pilot-operator;

\overline{C} —is the negative external condition affecting UAV landing in mountainous areas.

The mathematical expression of the criterion of adverse meteorological, atmospheric and environmental conditions can be described by Equation (18):

$$P(\overline{C}) \approx 0.12P(\overline{B}_0) \quad (18)$$

where:

P —is the probability of occurrence of an extraordinary situation;

\overline{C} —is the negative external condition affecting UAV landing in mountainous areas;

\overline{B}_0 —is the immediate negative influence that affects the chain UAV–pilot-operator.

The criterion expressed by Equation (18) presents the choice of the efficiency assurance criterion for ensuring the flight safety of the UAV–pilot-operator chain. Each criterion established in this way and based on the collection and evaluation of statistical data can be considered a set standard that can be used to ensure the flight safety of UAVs in all phases of flight in the mountains [17]. Thanks to applying this method (criteria) to the equation for the probability of occurrence of extraordinary situations (Equation (12)), the equation for estimating the probability of the occurrence of a complex UAV landing situation in the mountains (19) can be expressed as follows:

$$P_{ds} = 1 - P(B) \quad (19)$$

where:

P_{ds} —is the probability of occurrence of dangerous UAV states in the mountainous area;

P —is the probability of occurrence of an extraordinary situation;

B —is the influence that affects the chain UAV–pilot-operator.

Equation (19) can be used to estimate the probability of a dangerous (landing) UAV situation in the mountains, which can be expressed graphically (Figure 4) as a measure of the control factors of the changing flight parameters of a UAV moving in a specified space (mountain area) in the monitored time. Precisely, the time changes that arise during controlled landing as a posteriori projection of parameters can be mathematically written as several points in the n -dimensional Euclidean space E (20) [26–28]:

$$Z_{par}(t) = \alpha(t), MH(t), v(t), H(t), \dots, \omega_x(t), \omega_y(t), \omega_z(t) \quad (20)$$

where:

$Z_{par}(t)$ —is a set of possible flight parameters of the UAV in the determined mountain area in the monitored time;

$\alpha(t)$ —is the angle of attack of the UAV in the determined mountain area in the monitored time;

$MH(t)$ —is the magnetic heading of the UAV in the determined mountain area in the monitored time;

$v(t)$ —is the flight speed of the UAV in the determined mountain area in the monitored time;

$H(t)$ —is the flight height of the UAV in the determined mountain area in the monitored time;

$\omega_x(t)$ —is the X-axis position of the UAV in the determined mountain area in the monitored time;

$\omega_y(t)$ —is the Y-axis position of the UAV in the determined mountain area in the monitored time;

$\omega_z(t)$ —is the Z-axis position of the UAV in the determined mountain area in the monitored time.

These points can be sorted into classes, describing the characteristic zones of the UAV flight (Figure 4) within the scientifically and practically supported and tested corridor flight and the UAV approach to landing in a mountainous area, which was the subject of previous research by the authors [17,25].

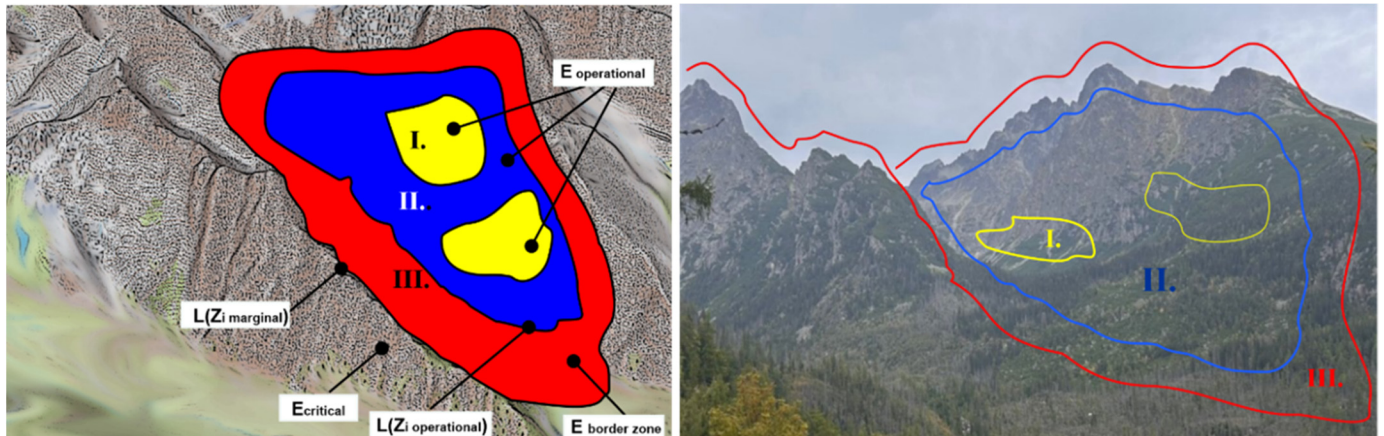


Figure 4. Profile of the distribution of acceptable UAV flight parameters when flying in a mountain environment (the Little Cold Valley, High Tatras, Slovak Republic). Legend: I.—the safe operational zone; II.—the acceptable operational zone; III.—the marginal operational zone, separated from the operating zone by a boundary band of permitted values.

The creation of zonal areas (Figure 4) represents the basis for the implementation and evaluation of UAV flight in a complex mountain environment, especially in the phase of the final approach to landing. Suppose the precise automated landing of the unmanned aerial vehicle in a designated mountain area with the help of the authors' landing system FDLS is considered. In that case, it is necessary to classify the flight parameters of the UAV—flight speed, flight height above the surrounding terrain, multiples of acceleration in all three axes, and the angle at which the UAV lands at the reference point SLA (the experimental landing area), based on the local/zonal area in which the approach to the landing area will occur.

The Euclidean area (zone) of acceptable operating values of UAV flight parameters (E_{op}) represents the sum of UAV flight parameters for which Equation (21) applies:

$$|Z_{ap}| \leq |Z_{np}| \quad (21)$$

where:

Z_{ap} —is the area (zone) in a mountainous environment in which acceptable UAV flight parameters may be exceeded;

Z_{np} —is the area (zone) in a mountainous environment with normal UAV flight parameters.

The Euclidean area (zone) of UAV flight parameter limit values (E_{bz}) is determined by Equation (22):

$$|Z_{mp}| < |Z_{ap}| \leq |Z_{np}| \quad (22)$$

where:

Z_{np} —is the area (zone) in a mountainous environment with normal UAV flight parameters;

Z_{ap} —is the area (zone) in a mountainous environment in which acceptable UAV flight parameters may be exceeded;

Z_{mp} —is the area (zone) in a mountainous environment with marginal UAV flight parameters.

The Euclidean area (zone) of critical values of UAV flight parameters (E_{cr}) represents UAV flight parameters reaching the critical limit, leading to an extraordinary and dangerous situation. This can be described by Equation (23):

$$|Z_i| > |Z_{i\ ma}| \quad (23)$$

where:

Z_{ap} —is the area (zone) in a mountainous environment in which acceptable UAV flight parameters may be exceeded;

Z_{mp} —is the area (zone) in a mountainous environment with marginal UAV flight parameters.

From the above, the level of criticality of the UAV flight in areas I, II, and III. (Figure 4) in the mountain environment of the researched (determined) area of the Little Cold Valley in the High Tatras can be determined. This area is defined by environmental influences (afforestation of the area; leeward and windward sides of the mountain massif) and atmospheric and meteorological influences (precipitation activity; the influence of the wind and mountain currents), as well as technical effects—a local area with losses of navigation signal from GNSS satellites—which significantly affect the flight of the unmanned aerial vehicle in this specific mountainous environment. The degree of riskiness of the UAV flight in the designated environment increases proportionally with worsening external conditions affecting the UAV flight—especially when approaching the uneven relief of a mountain massif, which creates unpredictable air vortex (Figure 4—zone III.).

The relations and equations mentioned above made it possible to create a complex simulation model in the MATLAB-Simulink environment, thanks to which it was possible not only to test the success of navigation of the UAV to the precise landing point even with the loss of GNSS navigation signals but also to take into account statistical indicators that create a timely prediction of the emergence of emergency situations.

As the loss of navigational signals is a significant factor in the prediction of mission failure or the destruction of the UAV due to its damage or catastrophe, the authors' collective dealt with the possibility of navigating the UAV in this specific determined area with an innovative ground-based landing system—frequency Doppler landing system (FDLS)—which will be explored in a separate article. The reliability and usability of FDLS technology were tested and evaluated in a simulation environment. Individual findings confirming the validity and usability of the newly designed FDLS technology will be presented in the following subsections and chapters.

2.3. Simulation and Evaluation Environment of the Success of a Simulated UAV Landing in a Mountainous Area Using the FDLS

To achieve our goal, we used the previously created unique universal workplace (Figure 5), which can be used for various tasks, such as the simulation of different UAVs and their flight in different environments and conditions and also for the evaluation and training of UAV pilot-operators for flight in these different conditions and situations. We can create flight scenarios that the UAV pilot-operator has to solve, and we can evaluate his success rate and, finally, his whole training process. The workplace consists of a simulation environment based on MATLAB—Simulink, where individual models of a UAV, environment, atmospheric conditions and scenarios could be set. For evaluation purposes, there is also the possibility to input commands by remote control.

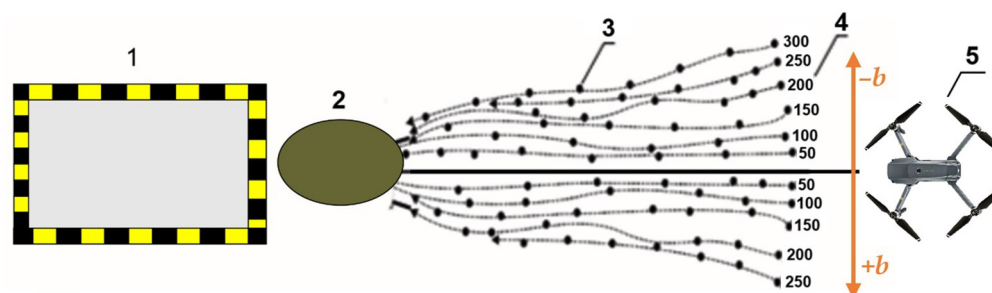


Figure 6. Graphical representation of the criterion of the UAV flying over the designated points—from the point of approach until the final landing on the experimental landing area. Legend: 1. experimental area for UAV landing in mountainous terrain; 2. frequency Doppler landing system (FDLS); 3. arrival lines (points) leading to the final landing point of the UAV; 4. the distance value from the central descent line (registered and evaluated by a microammeter, indicated in μA); 5. experimental unmanned aerial vehicle.

Selecting one of the criteria allows us to define the accuracy of the UAV descent with a specified probability. The method of simulation, experimental measurements and tests with statistical evaluation were used to solve the research task—the accuracy of landing at a specified point (experimental landing area) placed into a massif in the mountain environment. In order to determine the exact trajectories in the rugged mountain terrain, it was necessary to carry out a whole series of experimental measurements during the landing, thanks to which it was possible to collect and statistically evaluate information about the random errors of the unmanned aerial vehicle used as a supplementary UAV for the needs of HEMS, flying either fully autonomously or partially controlled by a pilot-operator [8–13,29–31].

The simulation environment was used to collect an extensive database of flying data. After processing the collected data, the success of navigating the UAV to land in the mountainous environment at an exact landing point using the navigation signals from the FDLS was evaluated at more than 95% (as will be described in the third chapter). This created a justified basis for the submission of an application for the issuance of a flight permit in the highly protected area of the Tatra National Park (TANAP). Based on the provided detailed statistics and analysis of the success of the simulation flights, this request was granted by the national authorities, with a term after the end of the 2023/2024 winter tourist season. It was thus possible to carry out a series of experimental flights directly in the highly protected area of the Little Cold Valley in the High Tatras. The justification for the national authorities' decision was the planned use of UAVs as supplementary devices for rescuing persons whose health and life are at risk provided by the mountain rescue service (MRS) and the helicopter medical rescue service (HEMS).

3. Results and Discussion

This chapter is focused on the realisation and statistical evaluation of the success of precision UAV landings using the FDLS in the mountainous area. Measurements of the characteristics of the accuracy of the UAV's position in the determined area were carried out under the random influence of the wind (in the simulation, it was a random change in wind speed and direction, statistically typical for the given area). The principle of solving the task was based on the method of evaluating the UAV navigation signals (position and height) measured in the determined position windows (corridors) with the acceptance of the errors of the respective systems. The resulting error represents the sum of all deviations from the determined descent trajectories (hypersurfaces) shown in the following figure (Figure 7).

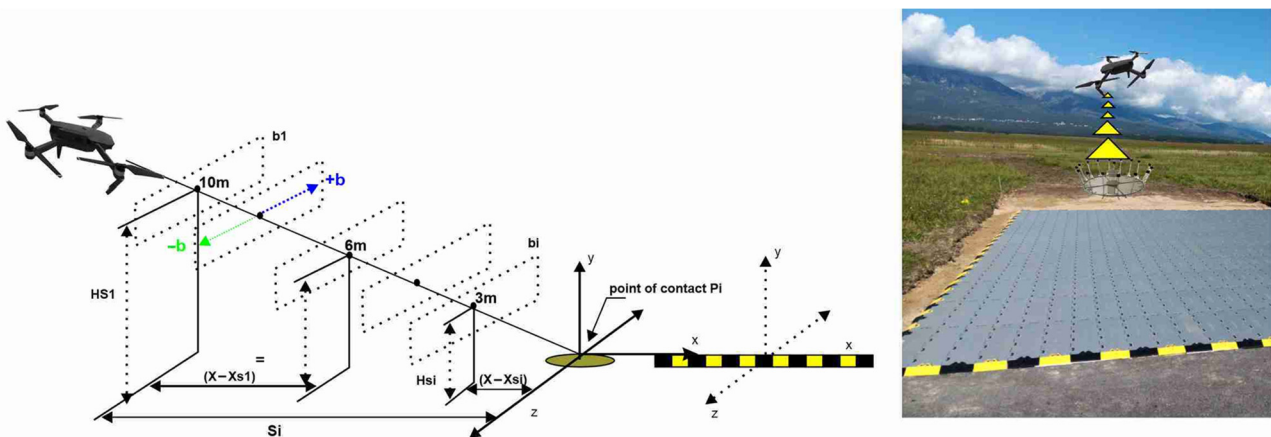


Figure 7. The position corridors define the limits of deviations from the nominal trajectory of the UAV position during landing, with the value of the descent plane angle $\Theta = 2.66^\circ$.

Where:

P_i —is the point of touch (interest) of the UAV at the experimental landing area;

b —is the horizontal width of the defined corridor (hypersurface);

b_i —is the defined corridor (hypersurface);

H —is the current flight height of the UAV above the terrain;

x_i —is the distance of the UAV's centre of gravity position from the point of touch (interest) at the experimental landing area;

z —is the lateral (horizontal) deviation from the ideal line (landing trajectory) of the UAV;

y —is the descent (vertical) deviation from the ideal line (landing trajectory) of the UAV;

S_i —is the ground distance between the actual position of the UAV and the point of touch (interest) placed at the experimental landing area located behind the FDLS.

Defined position windows (Figure 7) can be established in the time intervals of the UAV flight at specified distances (for example, 10 m, 6 m and 3 m). The mentioned options are determined by the mathematical hope (the mean value of the phenomenon that this variable represents) for the final approach of the UAV to the landing surface at the prescribed point P_i , located in front of the experimental landing area.

The evaluation analysis is aimed to obtain data for the statistics of UAV landing accuracy in a specific mountainous environment using the FDLS designed by the authors. The technical analysis follows the landing phase of the UAV flight in the airspace of the High Tatras region. A set of instrument components, course deviation indicators (CDIs), monitors the landing phase following the established rules for the relevant zone (Figure 4).

With a known number of measurements (in this research, it is 50 simulated flights/landings), values from the CDI are obtained, registered and compared in the form of a current measured by a microammeter. Based on the measured data, the curves (Figure 8) expressing the characteristics of the accuracy of the UAV landing in the mountainous area using the FDLS to the point of touch (interest) with the experimental landing area are compiled. The given curves represent the basis for recalculating the current data into a form suitable for displaying information about the horizontal and vertical deviation of the UAV from the ideal landing lines on the CDI display. This information also enters the UAV's autonomous control system or is displayed to the pilot-operator, who can lead the UAV to the landing point manually. The communication between the UAV and the FDLS is by radio link, which enables the exchange of information.

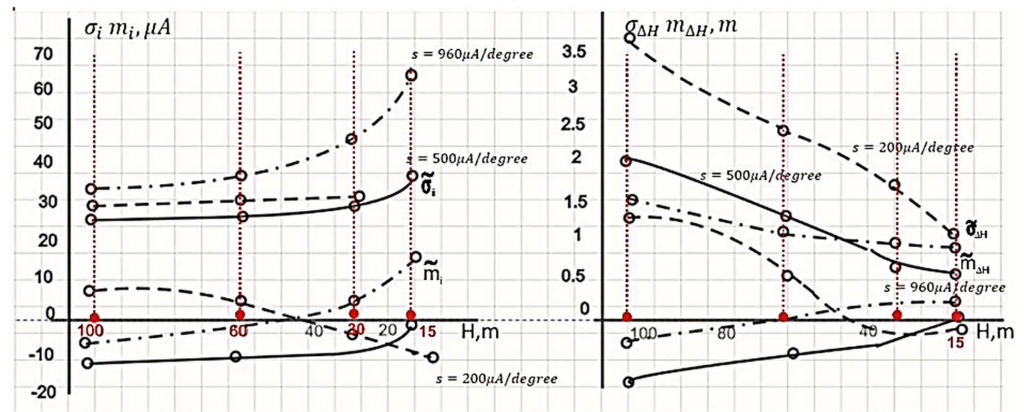


Figure 8. Characteristics of UAV descent accuracy in mountainous areas—information about the horizontal and vertical deviation of the UAV from the ideal landing point, used as a base for the course deviation indicator (CDI).

Observed and registered errors during the final approach to landing and the actual landing of the UAV in the mountain environment were evaluated from the point of view of the effectiveness of the required mission (landing). The statistical mechanism for the evaluation was the dispersion of the measurement error of the horizontal coordinate z at the time t (Equation (24)) and the dispersion of the error of the measured time t of the arrival of the UAV from the point of final approach of the UAV to the runway (Equation (25)) [26–28]:

$$D_z(t) = \sigma_z^2(t) \tag{24}$$

$$D_t(t) = \sigma_t^2(t) \tag{25}$$

where:

$D_z(t)$ —is the dispersion of the measurement error of the horizontal coordinate z at the time t ;

$D_t(t)$ —is the dispersion of the error of the measured time t ;

σ —is the root-mean-squared deviation.

For this reason, in order to calculate the efficient position when the UAV lands in the mountain massif, it is necessary to know the position windows (hypersurfaces) (Figure 7) and their distribution along the flight trajectory, as well as the correlation function of the longitudinal coordinate and the arrival time of the UAV to the destination point.

Positional windows (hypersurfaces) can be written in a simplified mathematical form as in Equation (26):

$$(x - x_s)^2 + (H - H_s)^2 + (z - z_s)^2 - S_i^2 = 0 \tag{26}$$

where:

$(x - x_s)$ —is the distance of the UAV’s centre of gravity position from the point of touch (interest) at the experimental landing area;

$(H - H_s)$ —is the current flight height of the UAV above the terrain;

$(z - z_s)$ —is the lateral (horizontal) deviation from the ideal line (landing trajectory) of the UAV;

S_i —is the ground distance between the actual position of the UAV and the point of touch (interest) placed at the experimental landing area located behind the FDLS.

According to the diagram in the figure (Figure 7), it is possible from the position of the defined corridor (hypersurface) in space (b_i) to define the following:

Disturbance caused by static errors—wind component constants, sensor errors and computing device errors.

Disturbances caused by dynamic errors—variable values of the wind component, high-frequency radio disturbances in the UAV deflection measurement circuits from the descent plane created by the FDLS, and imperfection and distortion of data from the landing system.

For the statistical evaluation of the success of the precise landing, taking into account static and dynamic errors as well as the characteristics of the used unmanned aerial vehicle and the designed FDLS (Table 1), the method of calculating the probability (P_1 and P_2) of a successful landing in the corridor (hypersurface) generated by the navigation FDLS is used. This statistical evaluation represents the degree of deviation of the UAV from the ideal landing line in the permitted corridor.

Table 1. The parameters used for simulation of UAV approach to landing area, SLA.

UAV flight speed during the final phase of the approach to landing and landing itself.	55 km/h
The time duration of the final phase of the approach to landing and the landing itself.	3 min = 180 s
The distance for interception and navigation of the UAV, with the navigation signals from the FDLS, for navigation to the final phase of the landing approach and the landing itself.	2.75 km = 2750 m
Permitted width of horizontal deviation ($\pm b$) of the UAV in the defined corridor (hypersurface) in the determined area—the Little Cold Valley, High Tatras.	± 3 m = ± 300 cm

Let P_1 be the probability of UAV movement at the level $+b$, i.e., from the ideal line of the landing corridor generated by the FDLS to the left of the ideal point of contact with the experimental landing area. Similarly, P_2 is the probability of UAV movement at the level $-b$, i.e., from the ideal line of the landing corridor generated by the FDLS to the right of the ideal point of contact with the experimental landing area. Calculations must be performed at the time of observation (experiment) $t = t_0 + \tau$. From this, Equations (27) and (28) can be set as follows [26–28]:

$$P_1 = f_1 \left[\frac{+b}{\sigma_z(t)} - (t_0 + \tau) \right] \quad (27)$$

$$P_2 = f_1 \left[\frac{-b}{\sigma_z(t)} - (t_0 + \tau) \right] \quad (28)$$

where:

P_1 —is the probability of UAV movement at the level $+b$, i.e., from the ideal line of the landing corridor generated by the FDLS to the left of the ideal point of contact with the experimental landing area;

P_2 —is the probability of UAV movement at the level $-b$, i.e., from the ideal line of the landing corridor generated by the FDLS to the right of the ideal point of contact with the experimental landing area;

f_1 —is a function of the standardised normal distribution;

b —is the horizontal width of the defined corridor (hypersurface);

σ —is the root-mean-squared deviation;

t_0 —is the initial time in the first section of the measurement;

τ —is the time shift in the measurement section.

The root-mean-square deviation σ_z , which is the square root of the dispersion $D_z(t)$ (Equation (24)), was used in the presented case. The polynomial $D_z(t)$ contains the measured values (time deviation from the ideal descent plane), sensor errors and their cross-correlations.

For the calculation and statistical evaluation of the probability P_1 (the probability of UAV movement at the level $+b$, i.e., from the ideal line of the landing corridor generated by the FDLS to the left of the ideal point of contact with the experimental corridor), there were 50 simulated flights and landings in the determined area of the Little Cold Valley. The time of the tracked final approach to landing and the landing itself, using the FDLS navigational signals, was set at three minutes (180 s). The measured values in the individual monitored corridors (hypersurfaces) were obtained by averaging ten measured samples for every second of the flight for each realised flight (a total of 90,000 samples). Subsequently, the data used to calculate the probability of deviation from the ideal descent trajectory were registered in the evaluation workplace of simulation flights (Figure 5). Graphical representation of the results of horizontal deviation to the left in the direction of flight of the UAV from the ideal line of the landing line, within the corridor (hypersurface) created by navigation signals from the FDLS, is shown in Figure 9.

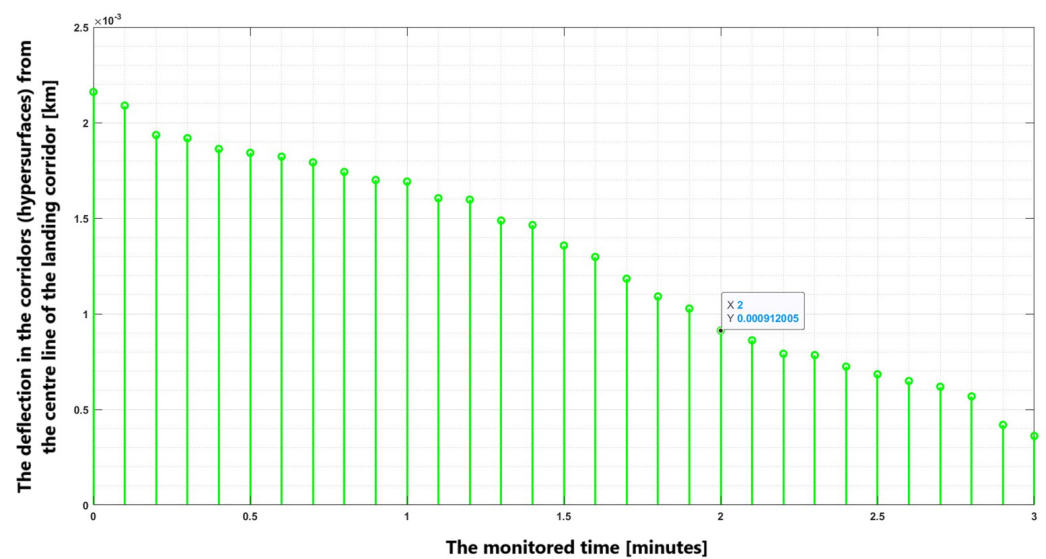


Figure 9. Graphical representation of the UAV deflection in the corridors (hypersurfaces) from the centre line of the landing corridor, determined by the FDLS navigation signals, to the left ($+b$) of the ideal point of contact with the experimental landing surface.

For the calculation and statistical evaluation of the probability P_2 (the probability of UAV movement at the level $-b$, i.e., from the ideal line of the landing corridor generated by the FDLS to the right of the ideal point of contact with the experimental landing area), there were 50 simulated flights and landings in the determined area of the Little Cold Valley. The time of the tracked final approach to landing and the landing itself, using the FDLS navigational signals, was set at three minutes (180 s). The measured values in the individual monitored corridors (hypersurfaces) were obtained by averaging ten measured samples for every second of the flight for each realised flight (a total of 90,000 samples). Subsequently, the data used to calculate the probability of deviation from the ideal descent trajectory were registered in the evaluation workplace of simulation flights (Figure 5). Graphical representation of the results of horizontal deviation to the left in the direction of flight of the UAV from the ideal line of the landing line, within the corridor (hypersurface) created by navigation signals from the FDLS, is shown in Figure 10.

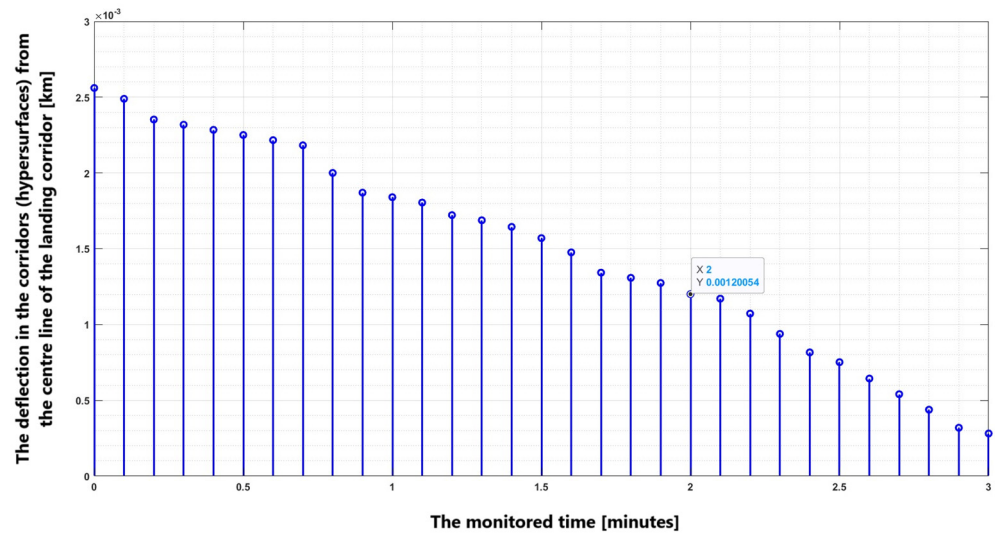


Figure 10. Graphical representation of the UAV deflection in the corridors (hypersurfaces) from the centre line of the landing corridor, determined by the FDLS navigation signals, to the right ($-b$) of the ideal point of contact with the experimental landing surface.

A three-dimensional graph (Figure 11) of the dependence of two primarily monitored flight variables (flight through the defined corridor (hypersurface) and height of the flight over the checkpoint) was created to present the measured data comprehensively. The three-dimensional area represents the experimental area for landing the UAV in a mountainous area using the FDLS navigation signals. The blue area is the coverage area of the FDLS radio navigation signals capturing receiving signals and evaluating equipment implemented onboard the UAV. The red segments represent the registered UAV deviation from the centre line of the landing corridor, shown in the previous figures (Figures 9 and 10), determined by the precise landing system FDLS.

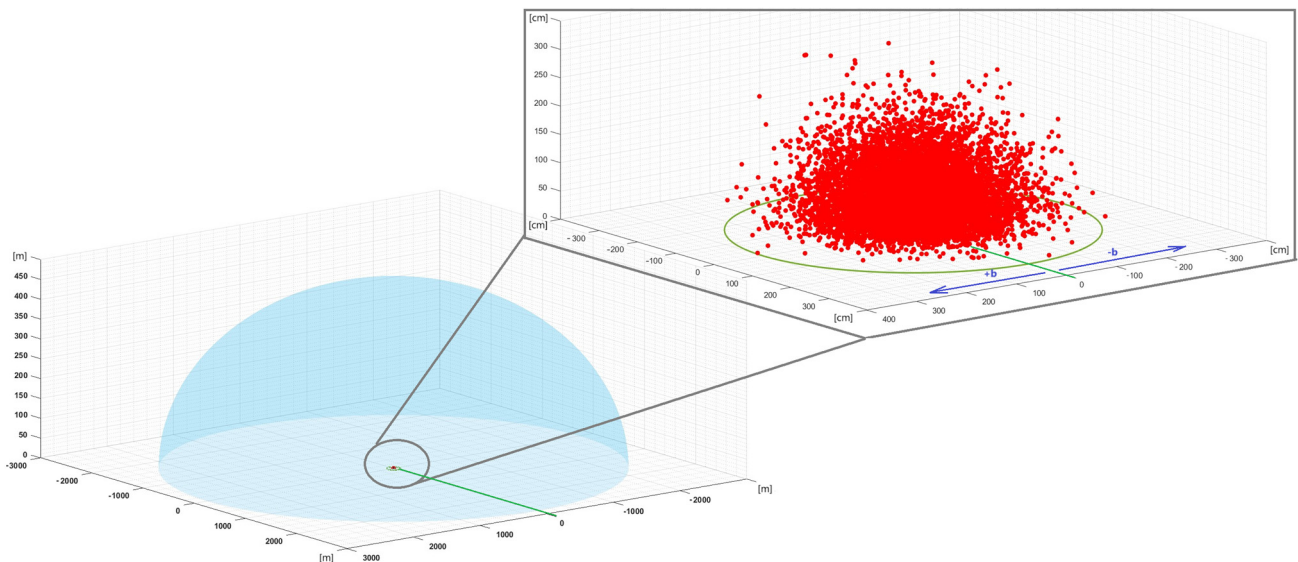


Figure 11. The three-dimensional presentation of the probability of UAV deviation from the ideal line of the landing corridor (hypersurface) created by FDLS's navigation signals.

The overall success of UAV flights and landings in a specific mountainous environment was evaluated by a feed-forward neural network with a finite number of neurons designed and trained by the authors. Selected neurons are connected, and individual connections between neurons have assigned values (weights). Subsequently, the neurons are arranged

in layers—one input layer, several hidden layers and one output layer. The task of the input layer is to receive input data for evaluating and training the network. The task of the output network is to interpret the results achieved by the network based on the supplied input data. The hidden layers process and transform the input data so the output layer can finally evaluate it [32].

The number of neurons used in individual layers and the interconnection of layers describes the neural network's architecture. This architecture uses so-called error backpropagation—based on changes in the values of synaptic weights calculated based on the error, where the error is considered to be the difference between the expected and the actual output of the neural network. Gradient methods are used to minimise this error [33,34]. To create subsequent training, testing and final verification of the neural network, the already mentioned series of measurements (fifty repetitions) of a simulated UAV flight and landing in a mountain environment using the FDLS navigation and landing system were used. The obtained data were sorted into three classes (1. successful landing, 2. partially successful landing and 3. unsuccessful landing) concerning the zone (Figure 4) where the flight was carried out. Due to the extensiveness of the database of measured and processed data, the final output of the trained and verified neural network used for evaluation purposes is shown in the form of a confusion matrix (Figure 12).

1	54900 61.0%	1620 1.8%	810 0.9%	95.8% 4.2%
2	450 0.5%	17100 19.0%	630 0.7%	94.1% 5.9%
3	990 1.1%	0 0.0%	13500 15.0%	93.2% 6.8%
	97.4% 2.6%	91.3% 8.7%	90.4% 9.6%	95.0% 5.0%
	1	2	3	

Figure 12. The confusion matrix—the results of the evaluation of the accuracy of the simulation flights and landings of the UAV in the mountainous area.

In the confusion matrix, the rows correspond to the predicted probability class (predicted landing success rate), the columns correspond to the actual class (actual landing success rate) and the diagonal cells (blue) correspond to observations with correct classification of success. Cells of the diagonals (orange) correspond to incorrectly classified

observations. In each cell, the number of observations and the corresponding percentage of the total observations are given.

The light grey column on the right side of the confusion matrix shows the percentage of all observations assumed to belong to a given class, regardless of whether they are correctly or incorrectly classified. It expresses the degree of accuracy (positive predictive value) and the rate of false deductions. The light grey row at the bottom of the confusion matrix shows the percentages of all observations belonging to each class, regardless of whether they are correctly or incorrectly classified. It is an expression of the rate of return (the rate of accurate positive response) and the rate of false (negative) responses. The green cell in the lower right corner of the confusion matrix shows the overall accuracy of evaluating the realised simulation measurements.

4. Conclusions

The use of unmanned aerial vehicles in mountainous areas has a number of specifics, especially when they are a part of supplementary devices for MRS and HEMS used to search for and rescue injured persons in hard-to-reach rugged terrain.

High mountains, especially mountain massifs, in addition to difficult environmental and atmospheric conditions, also create areas with GNSS signal losses, making accurate autonomous flights difficult and landing at the point of interest (SLA—successful landing area) in the mountain massif almost impossible. High-precision flight and precision landing are crucial for rescuing people in this specific environment. For this reason, the authors' team decided to create a high-precision navigation landing system, the FDLS (frequency Doppler landing system), whose simulation test of the success of UAV navigation to the landing point is the primary goal of the presented research and article.

A statistical evaluation of the success of the simulated flight/approach to the landing point and of the precise landing to the point of interest (successful landing area) using navigation signals from the FDLS itself was a condition of the national authorities of the Slovak Republic for the permission of experimental flights in the determined area of the High Tatras—the Little Cold Valley.

The overall evaluation of the success of the simulation flights and landings carried out under adverse atmospheric conditions (gusts of the wind; flight in the zone with the influence of the leeward and windward side of the mountain massif (Figure 4)), reached a 95% success rate (Figure 12). Under the mentioned hostile atmospheric conditions, there was a high success rate, as the landing accuracy of the unmanned aerial vehicle was lower than ± 50 cm (Figures 9–11).

Based on the statistical evaluation of the results, the future use of the FDLS in the mountain area can be predicted. The experimental flight tests in the determined area of the Little Cold Valley in the High Tatras are expected to occur in the second third of 2024. The following and connecting authors' research will be devoted to realising and evaluating experimental flights in a real mountainous environment of the Slovak High Tatras.

Author Contributions: Conceptualisation, P.K., N.G. and M.Č.; methodology, P.K., N.G. and M.Č.; software, N.G.; validation, N.G. and M.Č.; formal analysis, P.K., N.G. and M.Č.; investigation, N.G. and M.Č.; resources, P.K., N.G., M.Č. and A.Y.; data curation, P.K. and N.G.; writing—original draft preparation, P.K., N.G. and M.Č.; writing—review and editing, P.K., N.G. and M.Č.; visualisation, P.K., N.G. and M.Č.; supervision, P.K. and A.Y.; project administration, P.K., N.G. and A.Y.; funding acquisition, P.K., N.G., M.Č. and A.Y. All authors have read and agreed to the published version of the manuscript.

Funding: This research received no external funding.

Data Availability Statement: Data are contained within the article.

Acknowledgments: The work of N.G., P.K. and M.Č. was supported by the following project: KEGA 033TUKE-4/2023—Virtual Complex of Aircraft and Helicopter Systems as a Means of Supporting the Teaching of Avionics Subjects. The work of A.Y. was supported by the Fellowship for excellent

researchers threatened by the conflict in Ukraine (Project code: 09I03-03-V01-00060) within Slovakia's recovery and resilience plan funded by the European Union.

Conflicts of Interest: The authors declare no conflicts of interest.

References

1. ICAO Annex 14—Aerodromes. Available online: https://www.icao.int/safety/airnavigation/nationalitymarks/annexes_booklet_en.pdf (accessed on 8 September 2023).
2. Öktemer, E.; Gültekin, E.E. Operational usage and importance of instrument landing system (ILS). *Int. J. Aeronaut. Astronaut.* **2021**, *2*, 18–21.
3. Lopez, A.R. GPS Landing System Reference Antenna. *IEEE Antennas Propag. Mag.* **2010**, *52*, 104–113. [\[CrossRef\]](#)
4. Gross, J.N.; Gu, Y.; Rhudy, M.B. Robust UAV Relative Navigation with DGPS, INS, and Peer-to-Peer Radio Ranging. *IEEE Trans. Autom. Sci. Eng.* **2015**, *12*, 935–944. [\[CrossRef\]](#)
5. Felux, M.; Dautermann, T.; Becker, H. GBAS landing system—Precision approach guidance after ILS. *Aircr. Eng. Aerosp. Technol.* **2013**, *85*, 382–388. [\[CrossRef\]](#)
6. Cho, A.; Kang, Y.-S.; Park, B.-J.; Yoo, C.-S.; Koo, S.-O. Altitude integration of radar altimeter and GPS/INS for automatic takeoff and landing of a UAV. In Proceedings of the 11th International Conference on Control, Automation and Systems, Gyeonggi-do, Republic of Korea, 26–29 October 2011.
7. Klochan, A.E.; Al-Ammouri, A.; Dekhtyar, M.M.; Poleva, N.M. Fundamentals of the Polarimetric UAV Landing System. In Proceedings of the IEEE 5th International Conference Actual Problems of Unmanned Aerial Vehicles Developments (APUAVD), Kiev, Ukraine, 22–24 October 2019; pp. 153–156. [\[CrossRef\]](#)
8. Naidoo, Y.; Stopforth, R.; Bright, G. Development of an UAV for search & rescue applications. In Proceedings of the IEEE Africon '11, Victoria Falls, Zambia, 13–15 September 2011; pp. 1–6. [\[CrossRef\]](#)
9. Liu, Z.; Chen, H.; Wen, Y.; Xiao, C.; Chen, Y.; Sui, Z. Mode Design and Experiment of Unmanned Aerial Vehicle Search and Rescue in Inland Waters. In Proceedings of the 6th International Conference on Transportation Information and Safety (ICTIS), Wuhan, China, 22–24 October 2021; pp. 917–922. [\[CrossRef\]](#)
10. Ashish, M.; Muraleedharan, A.; CM, S.; Bhavani, R.R.; Akshay, N. Autonomous Payload Delivery using Hybrid VTOL UAVs for Community Emergency Response. In Proceedings of the IEEE International Conference on Electronics, Computing and Communication Technologies (CONECCT), Bangalore, India, 2–4 July 2020; pp. 1–6. [\[CrossRef\]](#)
11. Rudol, P.; Doherty, P. Human Body Detection and Geolocalization for UAV Search and Rescue Missions Using Color and Thermal Imagery. In Proceedings of the IEEE Aerospace Conference, Big Sky, MT, USA, 1–8 March 2008; pp. 1–8. [\[CrossRef\]](#)
12. ter Avest, E.; Kratz, M.; Dill, T.; Palmer, M. HEMS in mountain and remote areas: Reduction of carbon footprint through drones. *Scand. J. Trauma Resusc. Emerg. Med.* **2023**, *31*, 73. [\[CrossRef\]](#) [\[PubMed\]](#)
13. Claesson, A.; Fredman, D.; Svensson, L. Unmanned aerial vehicles (drones) in out-of-hospital-cardiac-arrest. *Scand. J. Trauma Resusc. Emerg. Med.* **2016**, *24*, 124. [\[CrossRef\]](#) [\[PubMed\]](#)
14. Yan, X.; Fu, T.; Lin, H.; Xuan, F.; Huang, Y.; Cao, Y.; Hu, H.; Liu, P. UAV Detection and Tracking in Urban Environments Using Passive Sensors: A Survey. *Appl. Sci.* **2023**, *13*, 11320. [\[CrossRef\]](#)
15. Salom, I.; Dimić, G.; Čelebić, V.; Spasenović, M.; Raičković, M.; Mihajlović, M.; Todorović, D. An Acoustic Camera for Use on UAVs. *Sensors* **2023**, *23*, 880. [\[CrossRef\]](#) [\[PubMed\]](#)
16. Yousaf, J.; Zia, H.; Alhalabi, M.; Yaghi, M.; Basmaji, T.; Shehhi, E.A.; Gad, A.; Alkhedher, M.; Ghazal, M. Drone and Controller Detection and Localization: Trends and Challenges. *Appl. Sci.* **2022**, *12*, 12612. [\[CrossRef\]](#)
17. Češkovič, M.; Kurdel, P.; Gecejová, N.; Labun, J.; Gamcová, M.; Lehocký, M. A Reasonable Alternative System for Searching UAVs in the Local Area. *Sensors* **2022**, *22*, 3122. [\[CrossRef\]](#) [\[PubMed\]](#)
18. Hussain, A.; Ahmed, A.; Shah, M.A.; Katyara, S.; Staszewski, L.; Magsi, H. On Mitigating the Effects of Multipath on GNSS Using Environmental Context Detection. *Appl. Sci.* **2022**, *12*, 12389. [\[CrossRef\]](#)
19. Iliiev, T.B.; Stoyanov, I.S.; Sokolov, S.A.; Beloev, I.H. The Influence of Multipath Propagation of the Signal on the Accuracy of the GNSS Receiver. In Proceedings of the 43rd International Convention on Information, Communication and Electronic Technology (MIPRO), Opatija, Croatia, 28 September–2 October 2020; pp. 508–511. [\[CrossRef\]](#)
20. Abdulkareem, A.; Oguntosin, V.; Popoola, O.M.; Idowu, A.A. Modeling and Nonlinear Control of a Quadcopter for Stabilization and Trajectory Tracking. *J. Eng.* **2022**, *2022*, 2449901. [\[CrossRef\]](#)
21. Wang, P.; Man, Z.; Cao, Z.; Zheng, J.; Zhao, Y. Dynamics modelling and linear control of quadcopter. In Proceedings of the 2016 International Conference on Advanced Mechatronic Systems (ICAMEchS), Melbourne, Australia, 30 November–3 December 2016. [\[CrossRef\]](#)
22. Ahmad, F.; Kumar, P.; Bhandari, A.; Patil, P.P. Simulation of the Quadcopter Dynamics with LQR based Control. *Mater. Today Proc.* **2020**, *24*, 326–332. [\[CrossRef\]](#)
23. Tagay, A.; Omar, A.; Ali, M.H. Development of control algorithm for a quadcopter. *Procedia Comput. Sci.* **2021**, *179*, 242–251. [\[CrossRef\]](#)
24. Quadcopter Flight Mechanics Model and Control Algorithms. Available online: https://wiki.control.fel.cvut.cz/mediawiki/images/5/5e/Dp_2017_gopalakrishnan_eswarmurthi.pdf (accessed on 1 October 2023).

25. Kurdel, P.; Češkovič, M.; Gecejová, N.; Adamčík, F.; Gamcová, M. Local Control of Unmanned Air Vehicles in the Mountain Area. *Drones* **2022**, *6*, 54. [[CrossRef](#)]
26. Onicha, J.N. *Advanced Mathematica*, 1st ed.; CreateSpace Independent Publishing Platform: Scotts Valley, CA, USA, 2014; pp. 131–243, 457–498.
27. Introduction to Mathematical Statistics. Available online: <https://minerva.it.manchester.ac.uk/~saralees/statbook2.pdf> (accessed on 10 October 2023).
28. Freund, J.E. *Mathematical Statistics with Applications*, 8th ed.; Pearson: London, UK, 2012; pp. 61–112.
29. Seier, G.; Hödl, C.; Abermann, J.; Schöttl, S.; Maringer, A.; Hofstadler, D.N.; Pröbstl-Haider, U.; Lieb, G.K. Unmanned aircraft systems for protected areas: Gadgetry or necessity. *J. Nat. Conserv.* **2021**, *64*, 126078. [[CrossRef](#)]
30. Píkov, V.; Ryapukhin, A.; Veas Iniesta, D. Information Protection in Complexes with Unmanned Aerial Vehicles Using Moving Target Technology. *Inventions* **2023**, *8*, 18. [[CrossRef](#)]
31. Kang, H.; Joung, J.; Kim, J.; Kang, J.; Cho, Y.S. Protect Your Sky: A Survey of Counter Unmanned Aerial Vehicle Systems. *IEEE Access* **2020**, *8*, 168671–168710. [[CrossRef](#)]
32. Ripley, B.D. Feed-forward Neural Networks. In *Pattern Recognition and Neural Networks*, 1st ed.; Cambridge University Press: Cambridge, UK, 1996; pp. 143–180. [[CrossRef](#)]
33. Aggarwal, C.C. *Neural Networks and Deep Learning*, 1st ed.; Springer: Cham, Switzerland, 2018; pp. 1–104. [[CrossRef](#)]
34. Dobeš, M.; Andoga, R.; Főző, L. Sensory integration in deep neural networks. *Acta Polytech. Hung.* **2021**, *18*, 245–254. [[CrossRef](#)]

Disclaimer/Publisher’s Note: The statements, opinions and data contained in all publications are solely those of the individual author(s) and contributor(s) and not of MDPI and/or the editor(s). MDPI and/or the editor(s) disclaim responsibility for any injury to people or property resulting from any ideas, methods, instructions or products referred to in the content.